Available online at www.sciencedirect.com

ScienceDirect

Ceramics International 40 (2014) 2419–2425

CERAMICS INTERNATIONAL

www.elsevier.com/locate/ceramint

X-ray reflectivity and surface energy analyses of the physical and electrical properties of α-IGZO/GZO double active layer thin film transistors

Jia-Ling Wu[a], Han-Yu Lin[a], Bo-Yuan Su[a], Yu-Cheng Chen[a], Sheng-Yuan Chu[a,b,d,*], Ssu-Yin Liu[a], Chia-Chiang Chang[c], Chin-Jyi Wu[c]

[a]Department of Electrical Engineering, National Cheng Kung University, Tainan 70101, Taiwan
[b]Advanced Optoelectronic Technology Center, National Cheng Kung University, Tainan 70101, Taiwan
[c]Industrial Technology Research Institute, Mechanical and Systems Research Laboratories, Hsinchu 310, Taiwan
[d]Research Center for Energy Technology and Strategy (RCETs), National Cheng Kung University, Tainan 70101, Taiwan

Received 13 May 2013; received in revised form 30 July 2013; accepted 5 August 2013
Available online 29 August 2013

Abstract

In this research, bottom-gate thin film transistors (TFTs) of amorphous indium gallium zinc oxide (α-IGZO)-based active layers were grown by the radio-frequency sputtering technique. The device characteristics of two kinds of TFT structures, namely α-IGZO/GZO double active layer TFT and α-IGZO single active layer TFT, were compared. To explain the differences in the TFT performances of these different structures, X-ray reflectivity (XRR) and contact angles of the active layer were measured. The α-IGZO/GZO double active layer TFT exhibits superior device performance as compared to the other TFT structure because of its highest thin film density (5.87 g/cm^3), lowest surface roughness (1.89 nm), and largest surface energy (60.07 mJ/m^2). Also, the mechanisms of this double active layer to improve the device characteristics were systematically investigated. The improved saturation mobility, sub-threshold voltage, on/off current ratio, and trap density of the α-IGZO/GZO double active layer TFT were 18.92 cm^2 V^{-1} S^{-1}, 0.33 V/decade, 1.33×10^8, and 4.25×10^{12} eV^{-1} cm^{-2}, respectively, indicating the potential of this structure to be applied on large-area-flat-panel displays.

Keywords: IGZO/GZO double active layer TFT; Thin film density; Adhesion properties

1. Introduction

Display technologies have become an important part of the high-technology industry in recent years. Among them, amorphous Si (α-Si) based thin film transistors (TFTs), which can be integrated with TFT-LCD and backlight source modules, are used widely as the drivers of TFT-LCD modules, such as Active Matrix Liquid Crystal Displays (AMLCD) [1] and Active Matrix Organic Light Emitting Diode Displays (AMOLED) [2]. However, the low field-effect mobility (~1 cm^2 V^{-1} S^{-1}), high photo sensitivity (due to Si's low band gap of about 1.7 eV) and high deposition temperature become critical issues of the amorphous Si active layer in TFTs [3]. Additionally, the excited photo carriers (photo current effect) may cause the AMLCD and AMOLED arrays to become out of control because the band gap of α-Si is in the visible region. Recently, amorphous oxide semiconductors (AOS) such as amorphous In_2O_3:Ga_2O_3:ZnO (α-IGZO) have extensively been studied for application in display devices due to many advantages over conventional amorphous and polycrystalline silicon for use in the active layers of TFTs, including better electrical properties, lower temperature processing, and higher transparency [4,5]. In this regard, transparent amorphous oxide semiconductors (TAOS) have attracted more and more attention for application in AMLCD, AMOLED, and transparent flexible displays [6,7]. Although improvements in the device structure and reliability of α-IGZO TFTs are in demand, their fabrication process and deposition parameters are nearly optimized.

*Corresponding author at: Department of Electrical Engineering, National Cheng Kung University, No.1, University Road, Tainan City 701, Taiwan. Tel.: +886 6 275 7575x62381; fax: +886 6 234 548.
E-mail address: chusy@mail.ncku.edu.tw (S.-Y. Chu).

0272-8842/$ - see front matter © 2013 Elsevier Ltd and Techna Group S.r.l. All rights reserved.
http://dx.doi.org/10.1016/j.ceramint.2013.08.015

Kim et al. demonstrated that adding an optimized 50-Å active layer ITO between the α-IGZO active layer and SiO_2 dielectric layer could enhance the TFTs characteristics of the mobility (μ_{FE}), threshold voltage (V_{TH}), and off current (I_{OFF}) from 19.18 to 104 $cm^2\ V^{-1}\ S^{-1}$, −0.6 to 0.5 V, and 0.57 to 0.30 pA, respectively. They showed that TFT with the double active layer could have high mobility by using an ultra thin layer of ITO with high carrier density around the gate insulator interface because the charges are induced into the channel from the dielectric layer. Accordingly, the V_{TH} value could be lowered by using a thick oxide layer as a major active layer [8].

On the other hand, X-ray reflectivity (XRR) is known as a non-destructive analysis method for the characterization of thin film materials; in particular, the properties of the density, thickness, and roughness of the films can be simultaneously obtained [9]. To our best knowledge, there have been few XRR studies regarding oxide TFTs. Jeong et al. reported the effect of deposition pressure on α-IGZO TFTs by the RF sputtering technique. The thin film density and the surface roughness of α-IGZO thin films could be obtained by fitting with XRR analyses. It was found that not only the thin film density but also the TFT device performance of the α-IGZO active layer increased monotonously with a decreasing deposition pressure. When the deposition pressure was decreased from 5 mtorr to 1 mtorr, the thin film density, surface roughness of the α-IGZO active layer, μ_{FE}, sub-threshold voltage (*S.S.*) value, on/off current ratio ($I_{ON/OFF}$), and trap density (N_t) were improved from 5.50 to 6.27 g/cm^3, 1.54 to 0.77 nm, 11.4 to 21.8 $cm^2\ V^{-1}\ S^{-1}$, 0.87 to 0.17 V/decade, 1×10^7 to 6.8×10^7, and 2.4×10^{12} to $0.33\times10^{12}\ cm^{-3}$, respectively [10].

In addition, wettability and surface energy are another important issues of the thin films with respect to their adhesion properties. Cho et al. suggested that the wettability contact angle of the thin films can determine the adhesion ability with the neighboring layers and influence the electric devices' performance [11]. Kwong et al. reported that the hydrophilic properties of the thin films' surface could be enhanced by chemical and physical modifications, which could promote the surface energy and reduce the surface roughness, respectively [12]. However, few studies have focused on the wettability and the surface properties of α-IGZO thin films as well as their effects on the device performance, which is the motivation of this work.

Nevertheless, double active layer structure of the α-IGZO/ITO and α-IGZO/IZO application on TFTs still had some drawbacks. Because indium was expensive, toxic, and more brittle than ZnO:Al (AZO) and ZnO:Ga (GZO), which was not suitable to be used for flexible TFTs [13]. Compared to the covalent bond length of Zn–O, the variations in the covalent bond length of Al–O and Ga–O are 0.13 and 0.05 Å, respectively, and thus GZO has a smaller lattice deformation than that of AZO. Additionally, Ga is less reactive to be oxided than Al during the deposition [14]. Therefore, GZO is more suitable than AZO to replace ITO to fabricate the double active layer structure of the α-IGZO TFTs. In the present work, the performances of α-IGZO/GZO double active layer TFTs have been reported for the first time. Furthermore, the physical and electrical mechanisms of the proposed TFT structures were systematically investigated in terms of the thin film density, surface roughness, and surface energy according to the XRR and contact angle analyses. Experimental results show that the TFT performances of the α-IGZO/GZO TFT structures were better than those of α-IGZO TFT structures. This could be attributed to the higher thin film density, lower surface roughness, and higher surface energy of the α-IGZO/GZO double active layer thin films as compared with α-IGZO single active layer thin film structures.

2. Experimental procedure

Bottom-gate type TFTs are generally applied to commercial liquid crystal displays. In order to reduce the damage on the channel surface during deposition, the bottom gate structure was employed for the fabrication of the α-IGZO TFTs. Fig. 1 (a) and (b) shows the schematic diagrams of the bottom gate of α-IGZO/GZO double active layer (Sample I) and α-IGZO single active layer (Sample II) TFTs. The fabrication process was as follows. Before device fabrication, commercial ITO glass substrates were used as the gate electrodes and were cleaned by sequential ultrasonic treatment in detergent, deionized water, acetone, and isopropyl alcohol. A 50-nm AlN/150-nm HfO_2 double stacked dielectric layer was deposited on ITO glass substrates by an RF sputtering system. Subsequently, the α-IGZO/GZO double active layer and the α-IGZO single active layer were deposited in the same manner. 2-inch α-IGZO (In:Ga:Zn=1:1:1 mol%) and 3-inch GZO (98 wt% ZnO:2 wt% Ga_2O_3) with a purity of 99.99% were used as the targets. The distance between target and substrate

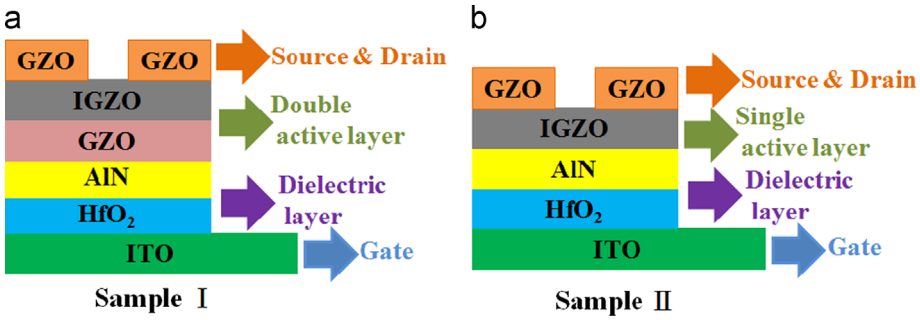

Fig. 1. Device structures of (a) α-IGZO/GZO double active layer TFTs (Sample I) and (b) α-IGZO single active layer TFTs (Sample II).

Table 1
The dielectric layer, active layer, and S/D electrode thin film of the deposition parameters.

Target material	HfO_2	AlN	GZO	α-IGZO	GZO
Use for	Dielectric layer	Dielectric layer	Single channel	Single& double channel	Source & drain
Ar/O_2 (sccm)	10.5/4.5	10/0	3/0.5	10/0	3/0
Base pressure (Torr)	$<6\times10^{-6}$	$<6\times10^{-6}$	$<6\times10^{-6}$	$<6\times10^{-6}$	$<6\times10^{-6}$
Working pressure (mTorr)	5	5	1	10	1
Target power setting (W)	150	100	30	60	30
Substrate temperature (°C)	Room temperature	Room temperature	Room temperature	Room temperature	Room temperature
Deposition time (min)	300	120	5	10	120
Thin film thickness (nm)	150	50	5	50	100
Distance between sputter target and substrate (cm)	7	7	7	7	7

was 7 cm and the base pressure was kept at 6×10^{-6} Torr. The GZO source and drain (S/D) electrodes of samples I and II were defined by metal shadow mask. 100-nm GZO layers as the S/D electrodes for all samples were further deposited by the RF sputtering technique. The channel width (W) and length (L) were 1000 and 100 μm, respectively. The deposition parameters of the dielectric layer, active layer, and S/D electrodes thin films are listed in Table 1.

Thicknesses of the thin films were determined by a surface profiler (Alpha-Step, KLA-Tencor, USA), while microstructure characteristics of the active layer thin films including the surface roughness and thin film density were analyzed by XRR. A standard θ–2θ X-ray diffraction (XRD) measurement was performed using CuKα radiation at 40 kV and 30 mA (D8 DISCOVER, Bruker Germany), the obtained data were fitted using the D8 DISCOVER Reflectivity Software package. In addition, the surface roughness of these active layer films were also confirmed by using atomic force microscopy (AFM) (di-CP II). The root-mean-square (rms) average surface roughness of these active layer films were calculated for a 3-μm^2 area.

For the surface measurement, the contact angles of the thin films' active layer were measured using the Sessile drop technique with a contact angle goniometer (MagicDrop, USA) under ambient conditions. Deionized (DI) water and methylene iodide ($C_2H_2I_2$) were used as the test liquids. A 3 μL drop of the solution was placed on the sample surface with a micropipette, the measurement of which was carried out after the drop reached metastable equilibrium (i.e., the process of spreading had stopped). An average of at least three measurements was performed for each data set. Their surface tensions, including polar (γ_L^p) and dispersion (γ_L^d) components, are in detail listed in Chen's work [15].

All of the TFTs electrical characteristics of the fabricated α-IGZO (Samples I and II) were measured by a semiconductor parameter analyzer (Agilent 4155C) in the dark at room temperature.

3. Results and discussion

The film density quality of the TFT active layer, which depends on the deposition parameters, can affect the TFT device performance. Thus, for estimating the active layer properties of all samples, the film density was analyzed by XRR. Usually, the surfaces of most thin-film materials are in the non-perfect condition because their surface roughness is not smooth enough. Many models have been proposed to explain the thin film growth mechanism. A straightforward model proposed by Als-Nielsen expresses the reflectivity of thin films from nonideal surfaces are detail presented in [9].

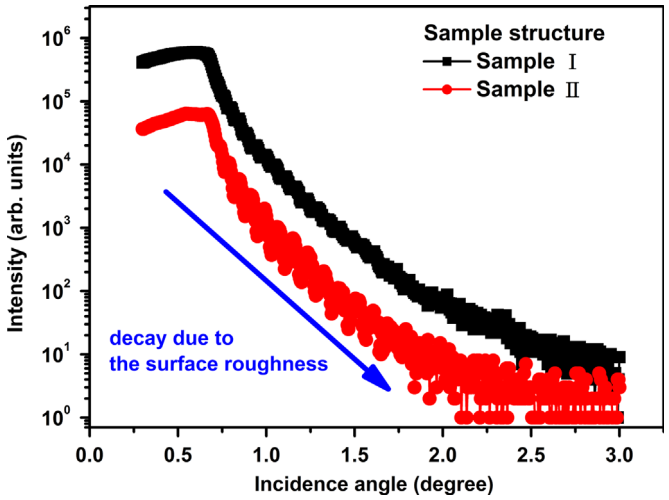

Fig. 2. The XRR figures of α-IGZO/GZO double active layer (Sample I) and α-IGZO single active layer (Sample II).

The measured active layer of the XRR figure and the fitting data of the thickness, surface roughness, and thin film density for Samples I and II are shown in Fig. 2 and Table 2, respectively. The possible mechanism can be explained as following. The critical angle for total external reflection for the α-IGZO/GZO double active layer is higher than that of α-IGZO single active layer, indicating that α-IGZO/GZO double active layer thin film was denser than α-IGZO single active layer thin film [16]. Additionally, the 5-nm GZO in α-IGZO/GZO double active layer thin film can be regarded as the buffer layer, which can make the active layer with lower surface roughness. As can be seen in Table 2, the roughness values exhibit a trend: Sample II (2.35 nm) > Sample I(1.89 nm). In addition, the trend exhibited in thin film density values shows Sample I (5.87 g/cm^3) > Sample II (5.25 g/cm^3). Fig. 3(a)–(b) shows the surface roughness topographies and plane view of the Samples I and II by AFM measurement,

respectively. From actual AFM measurement results, the surface roughness values of Sample II (Rms (rq)=2.198 nm) > Sample I (Rms (rq)=1.505 nm). This tendency is consisted with the XRR fitting results and provided the further evidences.

Table 2
The active layer of the XRR data of the thickness, surface roughness, and thin film density for the α-IGZO/GZO double active layer (Sample I) and α-IGZO single active layer (Sample II).

Active layer structure	Thickness (nm)	Surface roughness (nm)	Density (g/cm^3)
(Sample I)	50/5	1.89	5.87
(Sample II)	50	2.35	5.25

The surface energy of the films can be estimated by the measurement of the contact angles using the Owens–Wendt method [17]. Fig. 4 shows the surface energy data (γ_s) of the α-IGZO/GZO double active layer and α-IGZO single active layer, while the precise values of the surface energy data and contact angle values are presented in Table 3. γ_S^d and γ_S^p respectively represent the dispersion and polar components of γ_s, while θ is the contact angle. Note that, the γ_s parameters reflect the chemical properties of the surface, while the sum of γ_s^d and γ_s^p reveals the extent of hydrophilicity [18]. It is known that lower contact angle values indicate higher surface energy

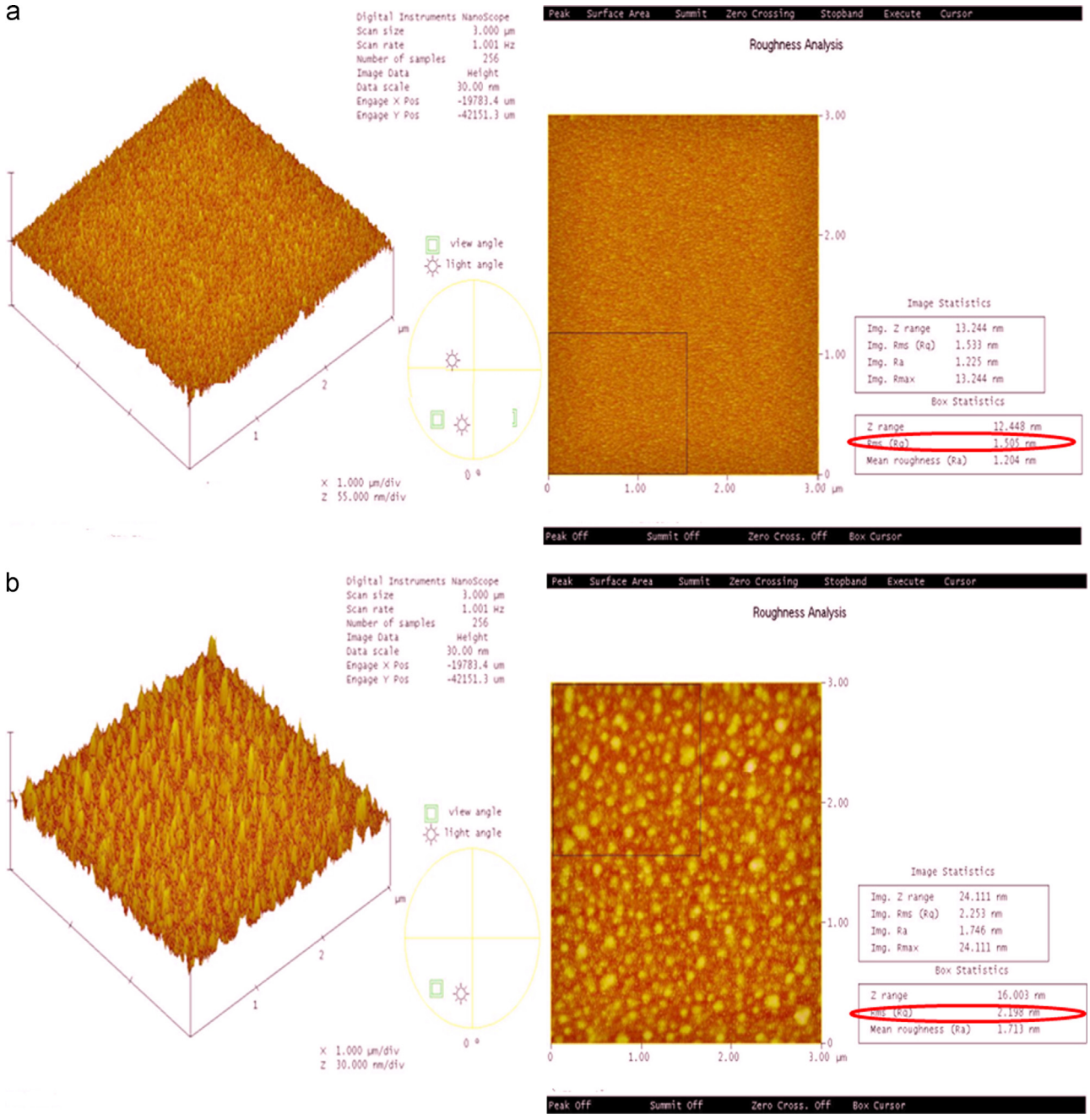

Fig. 3. The AFM topographies and plane view figures of (a) α-IGZO/GZO double active layer (Sample I) and (b) α-IGZO single active layer (Sample II).

[19]. Both the contact angle values of $C_2H_2I_2$ and H_2O exhibit the same trend: Sample I active layer < Sample II active layer. These results can be explained by two possible reasons, namely the surface roughness and surface energy effects. The contact angle can increase as the surface gets rougher [11,20,21], which matches well with the surface roughness data from the XRR fitting results listed in Table 2. The surface energy values exhibit the following trend: Sample I active layer (60.07 mJ/m^2) > Sample II active layer (46.81 mJ/m^2).It is known that a higher γ_s indicates higher hydrophilicity, and thus better adhesion at the surface [14,21,22]. Therefore, it can be concluded that the α-IGZO/GZO double active layer with the largest surface energy values has the best adhesion properties for deposition GZO S/D electrodes than α-IGZO single active layer.

TFTs with Sample I active layer and Sample II active layer were successfully fabricated. Fig. 5(a)–(c) illustrated the output [drain current vs. drain voltage (I_D–V_D)] and transfer [I_D vs. gate voltage (I_D–V_G) and $I_D^{1/2}$ vs. gate voltage ($I_D^{1/2}$–V_G) (at the fixed V_D of 40 V)] characteristics of Samples I and II TFTs, respectively. It shows that the device operates well in the n-channel enhancement mode. Since the channel layer is formed by the positive gate voltage, it is also observed that the drain current increases linearly with drain voltage at a low drain voltage, and exhibits clear pinch off voltage and current saturation at higher drain voltage. In general, the sub-threshold voltage (*S.S.*) values were defined as the gate voltage required to increase the drain current by a factor of 10, given by [7]

$$S.S. = \frac{dV_G}{d\log I_D} \tag{1}$$

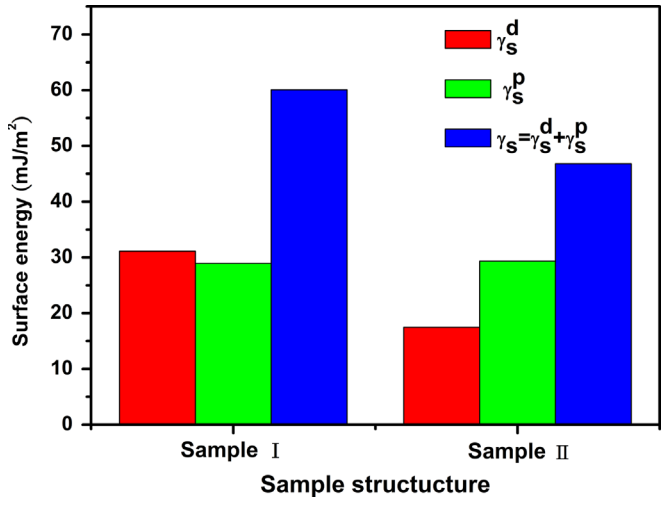

Fig. 4. The surface energy data (γ_s) of α-IGZO/GZO double active layer (Sample I) and α-IGZO single active layer (Sample II).

It shows that the *S.S.* value of Sample I (0.33 V/decade) < Sample II (0.69 V/decade). From the *S.S.* values, the maximum trap density (N_t) of the surface states at the interface between the channel and dielectric layer is approximated by the following equation [7]

$$N_t = \left[\frac{S\log(e)}{KT/q} - 1\right]\frac{C_i}{q} \tag{2}$$

where S is the sub-threshold slope (*S.S.*); k is the Boltzmann constant; T is the temperature; C_i is the gate insulator capacitance per unit area; and, q is the unit charge. All the device parameters extracted from these measured curves are listed in Table 4. It shows that N_t values of Sample II (9.64×10^{12} eV^{-1} cm^{-2}) > Sample I (4.25×10^{12} eV^{-1} cm^{-2}). Compared with Sample II TFT, Sample I TFT has a lower defect and less surface damage creation at or near the interface between the active layer and the dielectric layer [23,24].

The threshold voltage (V_{TH}) of these devices were obtained by fitting straight line of the square root of I_D vs. V_G. The saturation mobilities (μ_{sat}) were calculated as following equation:

$$I_d = \frac{C_{ox}\mu_{sat}W}{2L}(V_G - V_{TH})^2 \tag{3}$$

Where L and W are the active layer length and width, respectively, and C_{ox} is the capacitance of the gate insulator. Additionally, the rough surface and low thin film density can prohibit the transport of accumulated electrons and increase the scattering, and therefore increase the I_{OFF} current, leading to lower μ_{sat} of 5.64 cm^2 V^{-1} S^{-1}, higher *S.S.* values of 0.69 V/dec, worse V_{TH} of 6.09 V, and lower $I_{ON/OFF}$ ratios of 3.12×10^5 for Sample II. These results show that the improvement of μ_{sat} is correlated with the reduction of N_t and smoother surface morphology between the α-IGZO/dielectric layer interfaces. According to the surface roughness and thin film density of the XRR fitting results in Table 2, the double active layer structure was found to further suppress the defect creation of the α-IGZO single active layer structure TFT. Additionally, the TFT electric properties of Sample I were improved as compared with those of Sample II because of the increased thin film density, lower surface roughness, and higher surface energy of the active layer, as confirmed by the XRR and surface energy data in Tables 2 and 3.

In summary, the α-IGZO/GZO double active layer TFT has better performances than α-IGZO single active layer TFT, which is attributed by the following evidences: (1) the 5-nm GZO in α-IGZO/GZO double active layer was regarded as the buffer layer which can make the top α-IGZO film with lower surface roughness, increase the surface energy and promote the

Table 3
The active layer of the XRR data of the thickness, surface roughness, and thin film density for the α-IGZO/GZO double active layer (Sample I) and α-IGZO single active layer (Sample II). The surface energy data (γ_s) of α-IGZO/GZO double active layer (Sample I) and α-IGZO single active layer (Sample II).

Active layer structure	$C_2H_2I_2$ contact angle (degree)	H_2O contact angle (degree)	γ_s^p (mJ/m^2)	γ_s^d (mJ/m^2)	γ_s (mJ/m^2)
(Sample I)	36.06	38.3	28.95	31.12	60.07
(Sample II)	42.7	59	29.34	17.47	46.81

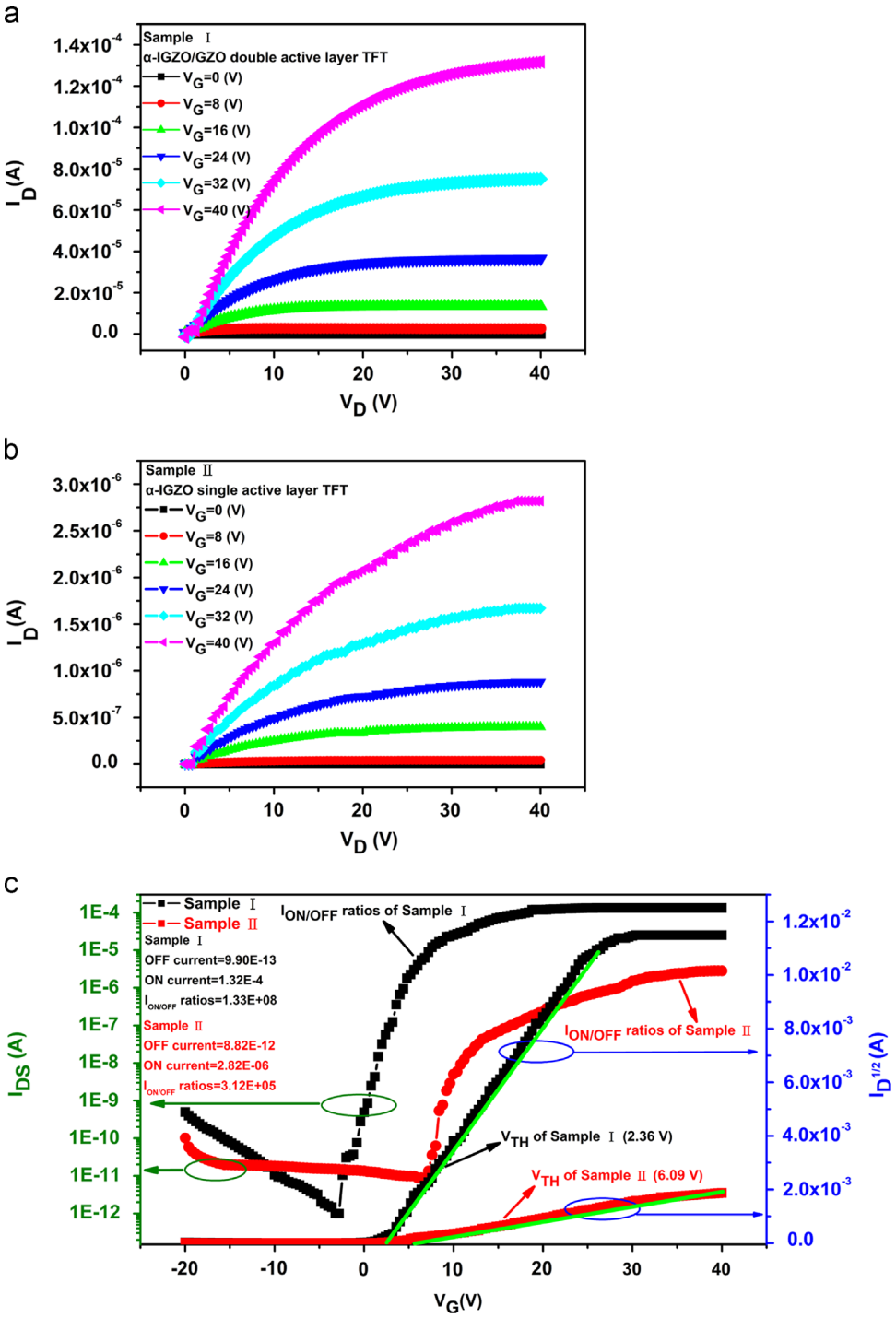

Fig. 5. Thin film transistors of output characteristics [drain current vs. drain voltage (I_D–V_D)] of (a) Sample I, (b) Sample II, and (c) transfer [I_D vs. gate voltage (I_D–V_G) and $I_D^{1/2}$ vs. gate voltage ($I_D^{1/2}$–V_G) (at the fixed V_D of 40 V)] characteristics of Samples I and II, respectively.

Table 4
TFTs device performance values of α-IGZO/GZO double active layer (Sample I) and GZO single active layer (Sample II).

TFT structure	μ_{sat} ($cm^2\ V^{-1}\ S^{-1}$)	*S.S.* (V/decade)	$I_{ON/OFF}$	V_{TH} (V)	N_t ($eV^{-1}\ cm^{-2}$)
(Sample I)	18.92	0.33	1.33×10^8	2.36	4.25×10^{12}
(Sample II)	5.64	0.69	3.12×10^5	6.09	9.64×10^{12}

GZO S/D electrodes adhesion ability, and thus can cause lower V_{TH} and higher I_{ON} currents of TFT device. (2) On the other hand, the α-IGZO/GZO double active layer with the higher thin film density than α-IGZO single active layer which can make the TFT device with lower N_t and smaller I_{OFF} currents and then increase the $I_{ON/OFF}$ ratios and μ_{sat}.

4. Conclusion

Enhancement-type α-IGZO-based TFTs were fabricated using AlN/HfO_2 and GZO transparent conductive oxide as the dielectric layer and electrodes, respectively. Two kinds of active layer structures, namely a double active layer of α-IGZO/GZO and single active layer of α-IGZO were studied. The α-IGZO/GZO active layer thin films were very stable and suitable for fabricating the thin film transistors because of its low surface roughness of 1.89 nm and high thin film density of 5.87 g/cm^3. Additionally, α-IGZO/GZO demonstrated the best adhesion properties to the neighboring thin film layers based on its high surface energy of 60.07 mJ/m^2. The μ_{sat}, *S.S.*, N_t, and $I_{ON/OFF}$ of the bottom-gate α-IGZO/GZO double-active layer devices characteristics were 18.92 cm^2 V^{-1} S^{-1}, 0.33 V/decade, 4.25×10^{12} eV^{-1} cm^{-2}, and 1.33×10^8, respectively. These results demonstrate that the α-IGZO/GZO double active layer TFT could be taken as a TFT structure candidate for application in large-area-flat-panel displays.

Acknowledgments

This work was supported by the National Science Council of Taiwan under Grants NSC 97-2221-E-006-241-MY3, NSC 100-3113-E-006–015, NSC 100-2120-M-006-001 and NSC 101-3113-E-006-014 and by the Display Technology Center, Industrial Technology Research Institute of Taiwan under Grant 100-C-073.

References

[1] C.Y. Liang, F.Y. Gan, P.T. Liu, F.S. Yeh, S.H. Chen, H.L. Chen, T.C. Chang, A novel self-aligned etch-stopper structure with lower photo leakage for AMLCD and sensor applications, IEEE Electron Device Letters 27 (2006) 978–980.

[2] B. Hekmatshoar, A.Z. Kattamis, K.H. Cherenack, K. Long, J.Z. Chen, S. Wagner, J.C. Sturm, K. Rajan, M. Hack, Reliability of active-matrix organic light-emitting-diode arrays with amorphous silicon thin-film transistor backplanes on clear plastic, IEEE Electron Device Letters 29 (2008) 63–66.

[3] Y.H. Tai, L.S. Chou, Y.F. Kuo, S.W. Yen, Gap-type a-Si TFTs for backlight sensing application, Journal of Display Technology 7 (2011) 420–425.

[4] W.F. Chung, T.C. Chang, C.S. Lin, K.J. Tu, H.W. Li, T.Y. Tseng, Y.C. Chen, Y.H. Tai, Oxygen-adsorption-induced anomalous capacitance degradation in amorphous indium–gallium–zinc-oxide thin-film-transistors under hot-carrier stress, Journal of the Electrochemical Society 159 (2012) H286–H289.

[5] Y.H. Tai, H.L. Chiu, L.S. Chou, The deterioration of a-IGZO TFTs owing to the copper diffusion after the process of the source/drain metal formation, Journal of the Electrochemical Society 159 (2012) J200–J203.

[6] S.K. Park, C.S. Hwang, M. Ryu, S. Yang, C. Byun, J. Shin, J. Lee, K. Lee, M.S. Oh, S. Im, Transparent and photo-stable ZnO thin-film transistors to drive an active matrix organic-light-emitting-diode display Panel, Advanced Materials 21 (2009) 678–682.

[7] E. Fortunato, P. Barquinha, R. Martins, Oxide semiconductor thin-film transistors: a review of recent advances, Advanced Materials 24 (2012) 2945–2986.

[8] S.I. Kim, C.J. Kim, J.C. Park, I. Song, S.W. Kim, H. Yin, E. Lee, J.C. Lee, and Y. Park, High Performance Oxide Thin Film Transistors with Double Active Layers, in: Proceedings of the Electron Devices Meeting, IEEE International, 2008.

[9] E. Chason, T.M. Mayer, Thin film and surface characterization by specular X-ray reflectivity, Critical Reviews in Solid State and Materials Sciences 22 (1997) 1–67.

[10] J.H. Jeong, H.W. Yang, J.S. Park, J.K. Jeong, Y.G. Mo, H.D. Kim, J. Song, C.S. Hwang, Origin of subthreshold swing improvement in amorphous indium gallium zinc oxide transistors, Electrochemical and Solid-State Letters 11 (2008) H157–H159.

[11] Y.C. Cho, S. Cha, J.M. Shin, J.H. Park, S.E. Park, C.R. Cho, S. Park, H. K. Pak, S. Jeong, A. Lim, The conversion of wettability in transparent conducting Al-doped ZnO thin film, Solid State Communications 149 (2009) 609–611.

[12] H.Y. Kwong, M.H. Wong, Y.W. Wong, K.H. Wong, Superhydrophobicity of polytetrafluoroethylene thin film fabricated by pulsed laser deposition, Applied Surface Science 253 (2007) 8841–8845.

[13] Y.S. Park, H.K. Kim, S.W. Kim, Thin Ag layer inserted GZO multilayer grown by roll-to-roll sputtering for flexible and transparent conducting electrodes, Journal of the Electrochemical Society 157 (2010) J301–J306.

[14] J.L. Wu, H.Y. Lin, Y.C. Chen, S.Y. Chu, C.C. Chang, C.J. Wu, Y.D. Juang, Effects of ZnO buffer layer on characteristics of ZnO:Ga films grown on flexible substrates: investigation of surface energy, electrical, optical, and structural properties, ECS Journal of Solid State Science and Technology, 2, P115–P119.

[15] Y.C. Chen, P.C. Kao, S.Y. Chu, UV-ozone-treated ultra-thin NaF film as anode buffer layer on organic light emitting devices, Optics Express 18 (2010) A167–A173.

[16] D.J. Kim, D.L. Kim, Y.S. Rim, C.H. Kim, W.H. Jeong, H.S. Lim, H.J. Kim, Improved electrical performance of an oxide thin-film transistor having multistacked active layers using a solution process, ACS Applied Materials and Interfaces 4 (2012) 4001–4005.

[17] A. Rudawska, E. Jacniacka, Analysis for determining surface free energy uncertainty by the Owen–Wendt method, International Journal of Adhesion and Adhesives 29 (2009) 451–457.

[18] H.J. Kim, J.W. Kim, H.H. Lee, T.M. Kim, J. Jang, J.J. Kim, Grazing incidence small-angle X-ray scattering analysis of initial growth of planar organic molecules affected by substrate surface energy, The Journal of Physical Chemistry Letters 2 (2011) 1710–1714.

[19] Y.C. Chen, Y.D. Juang, S.Y. Chu, P.C. Kao, Investigation of time-dependent UV-Ozone treatment on an ultra-thin AgF buffer layer for organic light-emitting diodes, Journal of the Electrochemical Society 159 (2012) H388–H392.

[20] J. Yang, J.K. Park, S. Kim, W. Choi, S. Lee, H. Kim, Atomic-layer-deposited ZnO thin-film transistors with various gate dielectrics, Physica Status Solidi A 209 (2012) 2087–2090.

[21] J.H. Cho, D.H. Lee, J.A. Lim, K. Cho, Evaluation of the adhesion properties of inorganic materials with high surface energies, Langmuir 20 (2004) 10174–10178.

[22] C.M. Wu, S.H. Su, H.T. Wang, M. Yokoyama, Morphology transformations of pentacene on an UV-patternable polymer insulator and their effect on performance of flexible organic thin-film transistors, Organic Electronics 13 (2012) 1962–1968.

[23] F. Zhou, H.P. Lin, L. Zhang, J. Li, X.W. Zhang, D.B. Yu, X.Y. Jiang, Z.L. Zhang, Top-gate amorphous IGZO thin-film transistors with a SiO buffer layer inserted between active channel layer and gate insulator, Current Applied Physics 12 (2012) 228–232.

[24] J.G. Um, M. Mativenga, P. Migliorato, J. Jang, Increase of interface and bulk density of states in amorphous-indium–gallium–zinc-oxide thin-film transistors with negative-bias-under-illumination-stress time, Applied Physics Letters 101 (2012) 113504-1–113504-4.